Singularity Loci and Kinematic Induced Constraints for an XY-Theta Platform Designed for High Precision Positioning

Anas Hijazi, Jean-François Brethe and Dimitri Lefebvre
Groupe de Recherche en Electrotechnique et Automatique du Havre (GREAH),
Le Havre University, BP540, 76058 Le Havre, France

Keywords: Singularity Analysis, Singular Surfaces, Jacobian Matrix, Redundant Manipulator Arm, XY-Theta Platform, Design and Kinematics.

Abstract: In this paper, the singularity analysis of an XY-Theta platform held by a serial redundant manipulator will be illustrated in details. This XY-Theta platform has a patented kinematics designed to keep the final position error below to 2 μm in its $300mm \times 300mm$ workspace (Hijazi et al., 2015). These high performances are obtained due to the combination of three factors: proximity to a singular configuration allowed by a specific choice of the arm lengths to reduce the lever arm lengths, redundant kinematic chain to enlarge the dexterous workspace and a two-step control using mechanical breaks set up on the furthest joints and exteroceptive sensors in the final step. However, if the proximity of singularities is useful for the precision performance, it may also cause some control problems. Consequently, it is crucial to identify the singularity loci and the kinematic constraints they induce. This analysis is done in two cases: when the first joint is considered locked and the robot is not redundant anymore and when the robot can be controlled using the four joints. In the non-redundant case, the usual singularity surface degenerates into an helix. In the redundant case, singularity surfaces may appear in specific configurations. In both cases, the induced kinematic constraints are analyzed and strategies are proposed to overcome the problems.

SCIENCE AND TECHNOLOGY PUBLICATIONS

1 INTRODUCTION

It is highly recommended to identify the singularities of a manipulator during the design stage, in order to be able to take into account their location for the control of the robot. Indeed, near singular configuration, the robot control algorithms may lead to large joint velocities or encounter instantaneous loss of dof (degree of freedom) (Merlet, 2006). This singularity analysis has been performed by many researchers on several different robots (Wenger, 2007),(Chablat and Wenger, 1998).

A robot has n dof in the operational space described by $\mathbf{x} = (x_1, ..., x_n)$ and m degrees of mobility in the actuator space described by $q = (q_1, ..., q_m)$. For serial robots, actuator and operational coordinates are linked by the forward kinematic function $\mathbf{x} = f(q)$. The Jacobian matrix appears after differentiating this relation: $d\mathbf{x} = Jdq$. Mathematically, considering the case of non-redundant serial robots, a loss of one or more dof is characterized by a drop in the rank of the Jacobian, implying $det(J) = 0$. If the serial robot is redundant, the location of the singularities are found using the following formula: $det(J \times J^T) = 0$ (Khalil and Dombre, 2002), (Tsai, 1999).

For parallel robots, the closed-form kinematic equations link the actuator and operational coordinates: $g(\mathbf{x}, q) = 0$ and two matrices A and B appear after differentiation:$A(\mathbf{x}, q)d\mathbf{x} + B(\mathbf{x}, q)dq = 0$. In (Gosselin and Angeles, 1990), Gosselin defined the serial and parallel singularities and proposed a classification of singularities into three types depending on the topology of the robot and the impact on the control:

1. Singularities of type I occur at the workspace boundaries and can be avoided by motion planning. This type named inverse kinematic singularity can be found in serial $det(J) = 0$ or parallel $det(B) = 0$ manipulators.
2. Singularities of type II result in additional dof at the end-effector and the mechanism cannot maintain its static equilibrium upon external forces. This type named direct kinematic singularity is specific to parallel manipulators.
3. Singularities of type III appear where both singularities of type I and II are present. Consequently

Hijazi, A., Brethe, J-F. and Lefebvre, D.
Singularity Loci and Kinematic Induced Constraints for an XY-Theta Platform Designed for High Precision Positioning.
DOI: 10.5220/0006827700390048
In *Proceedings of the 15th International Conference on Informatics in Control, Automation and Robotics (ICINCO 2018) - Volume 2*, pages 39-48
ISBN: 978-989-758-321-6
Copyright © 2018 by SCITEPRESS – Science and Technology Publications, Lda. All rights reserved

this type is also specific to parallel manipulators.

In (Merlet, 1989), Merlet proposed a new method based on Grassmann line-geometry to detect the singularities. Zlatanov thought that the role played by passive joint velocities was not utterly taken into account, and analyzed the problem in a more general way in (Zlatanov et al., 1995). He introduced the forward (FIKP) or the inverse (IIKP) instantaneous kinematic problems, interpreting singularities as a locus where the previous problems were undetermined. If the definitions of singularities seem now to cover a large spectrum of robot topology, it is still difficult to identify them. In some simple cases, analytical solutions can be found, but most of the time, numerical methods must be developed. For instance, in (Bohigasa et al., 2013) a numerical computation of manipulator singularities is presented. More research was realized by Malek to study the singularities in the presence of joint limits, concerning non-redundant robots (Abdel-Malek and Yeh, 2000) or even redundant robots (Mi et al., 2011).

In this paper, we study the singularity loci of an XY-Theta platform developed in our laboratory GREAH, designed to reduce the final position error below to 2 μm (Brethé, 2011b), (Hijazi et al., 2014), (Brethé et al., 2013). Our motivations to analyze the singularity loci of this platform are:

1. To know these undesirable postures of the singularity that should be recognized and avoided during the design, planning and control.
2. To operate the robot close to them to obtain a fine-positioning (Kao et al., 2007). In (Brethé, 2011a), it is shown that the spatial resolution and repeatability of a 2R plane serial robot is much better close to the center of the workspace, ie close to a singularity. The explanation is that the lever arm is short when the point lies near the singularity.

In section 2, the XY-Theta platform is presented in details. In section 3, the Jacobian matrix of the platform is calculated and the singularity configurations are analyzed. Then the singularity surfaces are drawn in the non-redundant and redundant cases. Finally, the conclusions are presented in section 4.

2 XY-Theta PLATFORM AND THE ROBOT PRECISION

2.1 Overview of the Platform Structure

The XY-Theta platform consists of a $300mm \times 300mm$ square and is held by a redundant kinematic chain of four motorized vertical revolute joints, with respective angles θ_1, θ_2, θ_3 and θ_4 displayed in Fig. 1. The first arm length is L_1 = 30 mm. The second and the third arm lengths are $L_2 = L_3$ = 120 mm. The prototype is displayed in Fig. 2.

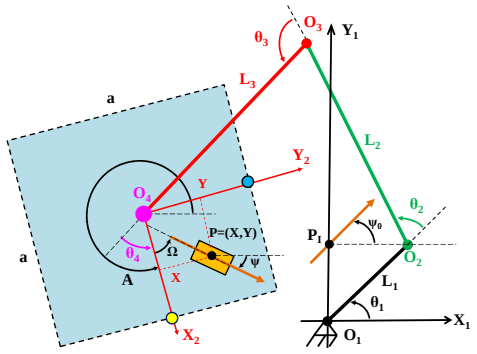

Figure 1: Diagram of the XY-Theta platform kinematics.

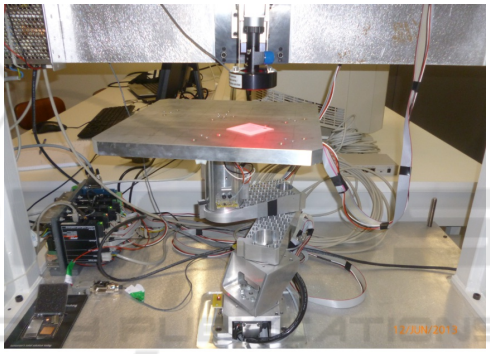

Figure 2: Micro positioning platform: general view.

This robot is designed to achieve precise positioning in the vicinity of a specific point named P_I "point of interest" in the workspace. $O_1P_IO_2$ is an isosceles, right-angled triangle when $\theta_1 = \frac{\pi}{4}$. The choice of this value is because the lever arm lengths between the first axis O_1 and the second axis O_2 from P_I are then minimum. These lengths can be calculated as: $O_1P_I = O_2P_I = L_1 \times \cos(\frac{\pi}{4}) = \frac{30}{\sqrt{2}} = 21.21mm$ and there are 6 times shorter than the second or third arm lengths of 120 mm. Moreover, the micro-movements induced by a micro-rotation of θ_1 and θ_2 are orthogonal.

There is an additional motorized vertical prismatic axis, which can hold a tool, for instance a gripper to grasp a workpiece. The vertical axis projection on the base lies at P_I. The robot is designed so that any workpiece on the platform can be picked and placed somewhere else on the platform with the desired orientation. Thus the operational space enables three degrees of freedom for the workpiece. To characterize the dof of the workpiece, the operational coordinates

$\mathbf{x} = (X, Y, \Omega)$ of the workpiece are given in the platform frame $(O_4X_2Y_2)$. $(O_1X_1Y_1)$ is the world frame coordinate system.

Let A be the rotation angle of the platform relative to the world frame:

$$A = \theta_1 + \theta_2 + \theta_3 + \theta_4 \tag{1}$$

Let Ψ be the the rotation angle of the workpiece relative to the world frame:

$$\Psi = A + \Omega \tag{2}$$

The gripper fixed on the vertical axis can grasp a workpiece when the workpiece center P lies at P_I with the specific orientation Ψ_0, sketched by the green arrow. Then we have necessarily: $A + \Omega = \Psi_0 \Rightarrow A = -\Omega + \Psi_0$.

2.2 The Coarse and Fine Positioning Modes

The platform can be operated in two different modes:

- The coarse positioning mode uses the four axes. In this case, the expected repeatability is in the range of 5-10 micrometers, which is equivalent to high quality industrial SCARA of the same reach.
- The fine positioning mode consists of two steps. In the first step, the workpiece is moved below the vertical axis at point P_I with the desired orientation using the four axes and θ_1 is set to $\frac{\pi}{4}$. Then, in the second step, the 3rd and 4th axes are blocked using mechanical brakes set up on these axes and the positioning error can then be reduced moving only the first and second axes. The choice of the blocked and moving axes depends on the lever arm length and from inception, the mechanism is designed to optimize the link lengths to reduce the final error. All points of the platform workspace can benefit from the high precision performance (Brethé et al., 2013),(Hijazi et al., 2014).

2.3 Kinematics Modeling

2.3.1 Forward Kinematics Function

The world $[WL]$ and platform $[PT]$ coordinates frames are here considered. The forward kinematics function links the actuator coordinates $\theta = (\theta_1, \theta_2, \theta_3, \theta_4)^T$ with the operational coordinates $\mathbf{x} = (X, Y, \Omega)^T$. The equations are the following:

$$\overrightarrow{O_1P} = \overrightarrow{O_1P_I} = \overrightarrow{O_1O_4} + \overrightarrow{O_4P_I} \tag{3}$$

$$\overrightarrow{O_1O_4}_{[WL]} = \begin{bmatrix} L_1.\cos(\theta_1) + L_2.\cos(\theta_1+\theta_2) + \overset{(1)}{L_3} \\ L_1.\sin(\theta_1) + L_2.\sin(\theta_1+\theta_2) + \overset{(2)}{L_3} \end{bmatrix} \tag{4}$$

Where $\overset{(1)}{L_3} = L_3.\cos(\theta_1+\theta_2+\theta_3)$ and $\overset{(2)}{L_3} = L_3.\sin(\theta_1+\theta_2+\theta_3)$. This matrix introduced in equation 4 will be named as: $B(\theta_1, \theta_2, \theta_3)$.

$$\overrightarrow{O_4P_I}_{[PT]} = \begin{bmatrix} X \\ Y \end{bmatrix} \tag{5}$$

$$\overrightarrow{O_4P_I}_{[WL]} = \begin{bmatrix} \cos(A) & -\sin(A) \\ \sin(A) & \cos(A) \end{bmatrix} \times \begin{bmatrix} X \\ Y \end{bmatrix}_{[PT]} \tag{6}$$

The matrix: $\begin{bmatrix} \cos(A) & -\sin(A) \\ \sin(A) & \cos(A) \end{bmatrix}$ will be named as $R(A)$.

$$\Omega = \Psi_0 - A \tag{7}$$

Once the four angles $(\theta_1, \theta_2, \theta_3, \theta_4)$ are given, the resolution of the equations leads to a unique solution.

2.3.2 Inverse Kinematic Modeling

The inverse kinematics model is used to calculate the joint coordinates θ in terms of the operational coordinates $\mathbf{x}$. The robot being redundant, there is an infinity of solutions.

Let us study the inverse kinematic function when θ_1 is set to $\pi/4$, so that the robot is not redundant anymore.

The coordinates of the point of interest P_I are:

$$P_I = \begin{bmatrix} 0 \\ L_1 \times \sin(\theta_1) \end{bmatrix} = \begin{bmatrix} 0 \\ L_1/\sqrt{2} \end{bmatrix} \tag{8}$$

The coordinates of O_4 can first be computed using the known angle $A = \Psi_0 - \Omega$.

$$O_4 = P_I + R(A) \times \begin{bmatrix} X \\ Y \end{bmatrix} \tag{9}$$

The coordinates of O_2 can easily be calculated as $\theta_1 = \pi/4$. Then θ_2 and θ_3 are the solutions of a usual geometric problem, consisting of connecting O_2 and O_4 with two links and two rotoid joints (inverse kinematics function of a 2R planar serial robot).

At this stage, θ_1, θ_2 and θ_3 are known and the desired orientation of the platform Ω is also known, so θ_4 can be deduced:

$$\theta_4 = \Psi_0 - \Omega - \theta_1 - \theta_2 - \theta_3 \tag{10}$$

We set now $\Psi_0 = 0$ so $\Omega = -(\theta_1 + \theta_2 + \theta_3 + \theta_4)$.

3 SINGULARITY ANALYSIS

In this section, singularity analysis of the XY-Theta is performed, based on the Jacobian of the manipulator. In our case, a serial robot is studied, so a singularity of the first type presented by Gosselin (Gosselin and Angeles, 1990) will be expected. XY-Theta platform is a kinematic chain consisting of a set of rigid bodies connected to each other with joints. This chain is also characterized by a set of inputs corresponding to the 4-dimensional vector $\theta = (\theta_1, \theta_2, \theta_3, \theta_4)$ of the actuated joints, and by a set of output coordinates corresponding to an 3-dimensional vector $\mathbf{x} = (X, Y, \Omega)$. The relation between the input and output coordinates is:

$$\mathbf{x} = f(\theta) \tag{11}$$

3.1 Jacobian Matrix

By differentiating Eq. 11 with respect to time and defining the Jacobian matrix as $J = df/d\theta$ the following equation is obtained:

$$\dot{\mathbf{x}} = J(\theta) \times \dot{\theta} \tag{12}$$

Eq. 3 and 8 lead to Eq. 13.

$$\begin{bmatrix} 0 \\ L_1/\sqrt{2} \end{bmatrix} = B(\theta_1, \theta_2, \theta_3) + R(A) \times \begin{bmatrix} X \\ Y \end{bmatrix} \tag{13}$$

By solving Eq. 13, the coordinates (X, Y, Ω) are obtained with Eq. 14 and 15.

$$\begin{bmatrix} X \\ Y \end{bmatrix} = R(A)^{-1} \times \begin{bmatrix} 0 \\ L_1/\sqrt{2} \end{bmatrix} - R(A)^{-1} \times B(\theta_1, \theta_2, \theta_3) \tag{14}$$

$$\Omega = -A = -(\theta_1 + \theta_2 + \theta_3 + \theta_4) \tag{15}$$

Therefore in the general case, the Jacobian matrix will be composed of four columns:

$$J = \begin{bmatrix} \vec{J}_1 \vec{J}_2 \vec{J}_3 \vec{J}_4 \end{bmatrix} \tag{16}$$

3.1.1 Non-redundant Case

Here, θ_1 is set to $\pi/4$ as presented in section 2 so the robot is not redundant. In this case the Jacobian is given by:

$$\begin{bmatrix} \dot{X} \\ \dot{Y} \\ \dot{\Omega} \end{bmatrix} = \overset{(1)}{J}(\theta) \cdot \begin{bmatrix} \dot{\theta_2} \\ \dot{\theta_3} \\ \dot{\theta_4} \end{bmatrix} \tag{17}$$

$$\overset{(1)}{J}(\theta) = \begin{pmatrix} \frac{\partial}{\partial\theta_2}(X) & \frac{\partial}{\partial\theta_3}(X) & \frac{\partial}{\partial\theta_4}(X) \\ \frac{\partial}{\partial\theta_2}(Y) & \frac{\partial}{\partial\theta_3}(Y) & \frac{\partial}{\partial\theta_4}(Y) \\ \frac{\partial}{\partial\theta_2}(\Omega) & \frac{\partial}{\partial\theta_3}(\Omega) & \frac{\partial}{\partial\theta_4}(\Omega) \end{pmatrix} = \begin{bmatrix} \vec{J}_2 \vec{J}_3 \vec{J}_4 \end{bmatrix} \tag{18}$$

3.1.2 Redundant Case

Here, the four arms of the robot are free to move. In this case the Jacobian is given by:

$$\begin{bmatrix} \dot{X} \\ \dot{Y} \\ \dot{\Omega} \end{bmatrix} = \overset{(2)}{J}(\theta) \cdot \begin{bmatrix} \dot{\theta_1} \\ \dot{\theta_2} \\ \dot{\theta_3} \\ \dot{\theta_4} \end{bmatrix} \tag{19}$$

$$\overset{(2)}{J}(\theta) = \begin{pmatrix} \frac{\partial}{\partial\theta_1}(X) & \frac{\partial}{\partial\theta_2}(X) & \frac{\partial}{\partial\theta_3}(X) & \frac{\partial}{\partial\theta_4}(X) \\ \frac{\partial}{\partial\theta_1}(Y) & \frac{\partial}{\partial\theta_2}(Y) & \frac{\partial}{\partial\theta_3}(Y) & \frac{\partial}{\partial\theta_4}(Y) \\ \frac{\partial}{\partial\theta_1}(\Omega) & \frac{\partial}{\partial\theta_2}(\Omega) & \frac{\partial}{\partial\theta_3}(\Omega) & \frac{\partial}{\partial\theta_4}(\Omega) \end{pmatrix} \tag{20}$$

3.2 Singular Surfaces

3.2.1 Non-redundant Case

In this case, the serial manipulator presents singularities of type I named boundary or interior singularities (Tsai, 1999),(Khalil and Dombre, 2002). Boundary singularities appear when the manipulator is fully stretched out, interior singularities when the manipulator is folded back on itself. The boundary and interior singularities can therefore be determined from the analytical expression of the determinant:

$$det(\overset{(1)}{J}(\theta)) = 0 \tag{21}$$

The solutions of this equation are: $S_1 = \{\theta_3 = 0\}$, $S_2 = \{\theta_3 = \pm\pi\}$.

The singular configuration S_1 is displayed in Fig. 3 when the third arm L_3 is fully stretched out and second one S_2 is displayed in Fig. 4 when the third arm L_3 is folded back on itself.

Let us draw the boundary singularity surface when $\theta_3 = 0$. The conditions are the following: $\theta_1 = \pi/4$, $-\pi \leq \theta_2 \leq \pi$, $-\pi \leq \theta_4 \leq \pi$. The singularity surface in red is displayed in Fig. 6. Let us draw the interior singularity surface in blue when $\theta_3 = \pi$. The conditions are the following: $\theta_3 = \pi$, $-\pi \leq \theta_2 \leq \pi$ and $-\pi \leq \theta_4 \leq \pi$. The singularity surface is also displayed in Fig. 5 and Fig. 6.

In this particular case, the singularity locus is not a surface anymore but it is an helix of radius $O_4P_I = L_1 \times \cos(\frac{\pi}{4}) = \frac{30}{\sqrt{2}} = 21.21mm$ and pitch 2π. This case

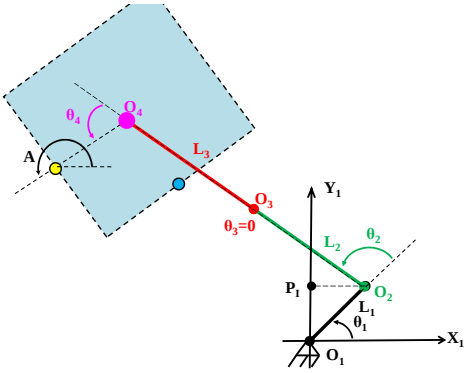

Figure 3: Singularity configurations corresponding to S_1 when $\theta_3 = 0$.

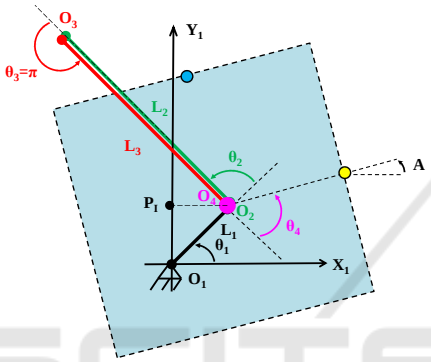

Figure 4: Singularity configurations corresponding to S_2 when $\theta_3 = \pi$.

is unusual and it is worth explaining its origin and the specific kinematic problems linked to this.

Usually in a 3D output space, the singularity locus is a surface. Here it is only a line. This phenomenon occurs because the lengths of the 2nd and 3rd arm are identical $L_2 = L_3 = 120[mm]$. If these lengths were different, the singularity locus would be a surface delineating an helicoidal cylinder. The end-effector (EE) could not go in the interior of this helicoidal cylinder because it would be outside the workspace. This is clearly illustrated in Fig. 7 where the helicoidal cylinders are drawn for different lengths of L_3, L_2 being constant at $120[mm]$.

The radius of the cylinder section in the XY plane is equal to $|L_3 - L_2|$. When $L_2 = L_3$ the helicoidal cylinder degenerates into an helix. The underlying question is then the following: as the volume of this helix is nil, can we consider that the workspace is plain? In fact, this is the case because the EE can be anywhere, but when the EE lies on the helix locus, some control problems occur which will be now described in detail.

First, let us prove that $\vec{J}_2$ is always tangent to the helix. For this, let us consider that the platform is stationary as detailed in Fig. 8.

The mechanism has then four actuated revolute

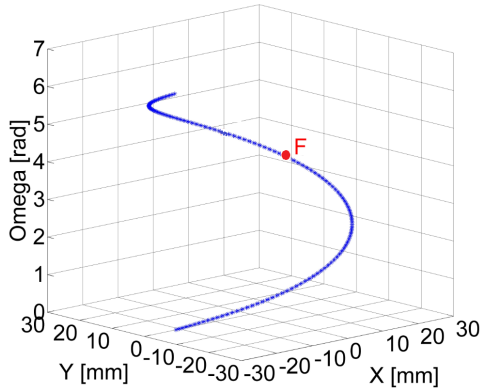

Figure 5: Singularity curve when $\theta_3 = \pi$.

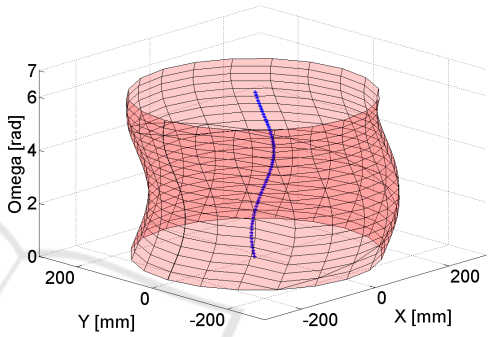

Figure 6: Singularity surface and singularity curve when the robot is non-redundant.

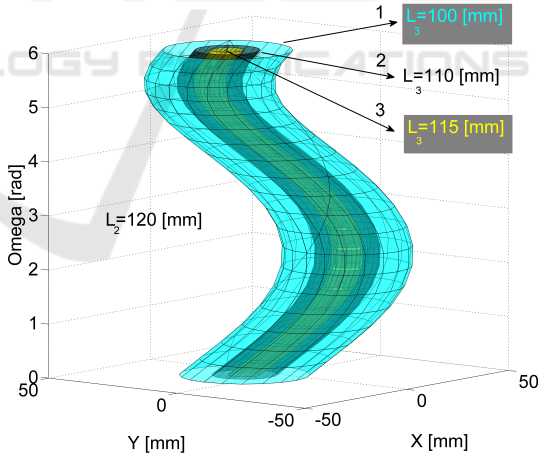

Figure 7: Workspace evolution when L_2 and L_3 are different.

joints and the forward kinematics function can be expressed as:

$$\begin{aligned} X &= L_3\cos(\pi-\theta_4)+L_2\cos(\pi-\theta_4-\theta_3)+C \\ Y &= L_3\sin(\pi-\theta_4)+L_2\sin(\pi-\theta_4-\theta_3)+D \\ \Omega &= -\theta_4-\theta_3-\theta_2-\theta_1 \end{aligned} \quad (22)$$

where $L_0 = L_1/\sqrt{2}$, $C = L_1\cos(\pi-\theta_4-\theta_3-\theta_2) + X_x$, $D = L_1\sin(\pi-\theta_4-\theta_3-\theta_2) + Y_y$, $X_x =$

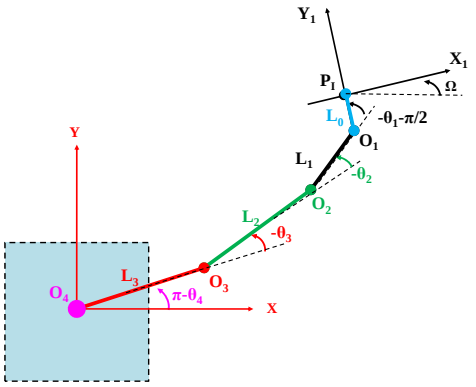

Figure 8: kinematics of the planar robot considering the platform stationary.

$L_0\cos(\pi-\theta_4-\theta_3-\theta_2-\theta_1-\pi/2)$ and $Y_y = L_0\sin(\pi-\theta_4-\theta_3-\theta_2-\theta_1-\pi/2)$.

The locus of singularity corresponds to $\theta_1 = \pi/4$ and $\theta_3 = \pi$. As $L_2 = L_3$, after simplification, the equations are the following:

$$s = \begin{bmatrix} X = L_0\cos(\theta_4+\theta_2+\pi/4) \\ Y = -L_0\sin(\theta_4+\theta_2+\pi/4) \\ \Omega = -\theta_4-\theta_3-\theta_2-\theta_1 \end{bmatrix} \quad (23)$$

We recognize here the equations of an helix which can be parametrized with $a = \theta_2+\theta_4$. The tangent vector to the helix is obtained by differentiating the previous equation and leads to the vector $t = \partial s/\partial a$:

$$t = \begin{bmatrix} -L_0\sin(a+\pi/4) \\ L_0\sin(a-\pi/4) \\ -1 \end{bmatrix} \quad (24)$$

On the other hand, after differentiating the forward kinematic function expressed in Eq. 22 with respect to θ_2, the expression of $\vec{J}_2$ is obtained:

$$\vec{J}_2 = \begin{bmatrix} L_0\sin(\pi/2-\theta_1-\theta_2-\theta_3-\theta_4)-G \\ L_1\cos(-\theta_2-\theta_3-\theta_4)-H \\ -1 \end{bmatrix} \quad (25)$$

Where $G = L_1\sin(-\theta_2-\theta_3-\theta_4)$ and $H = L_0\cos(\pi/2-\theta_1-\theta_2-\theta_3-\theta_4)$.

Then on the helix, setting $\theta_1 = \pi/4$ and $\theta_3 = \pi$, the value of $\vec{J}_2$ is the following:

$$\vec{J}_2 = \begin{bmatrix} -L_0\sin(\theta_2+\theta_4+\pi/4) \\ L_0\sin(\theta_2+\theta_4-\pi/4) \\ -1 \end{bmatrix} \quad (26)$$

It can be seen that $t(a=\theta_2+\theta_4) = \vec{J}_2(\theta_1=\pi/4,\theta_2,\theta_3=\pi,\theta_4)$ and consequently $\vec{J}_2$ is tangent to the helix.

When $L_2 = L_3$ and $\theta_3 = \pi$, the centers of axes 2 and 4 lie on the same point, thus the velocities vectors $\vec{J}_2$ and $\vec{J}_4$ are identical. The velocity vector $\vec{J}_3$ is always different from $\vec{J}_2$. For every point on the helix, there is an infinity of solutions verifying $\theta_2+\theta_4 = constant$.

For instance, let us consider the point F on the helix corresponding to $\{\theta_1 = \pi/4, \theta_2 = -\pi/4, \theta_3 = \pi, \theta_4 = 0\}$. The coordinates of F in the output space is $\{X = 21.21[mm], Y = 0[mm], \Omega = \pi[rad]\}$. All combinations $\theta_2+\theta_4 = -\pi/4$ will give the same location $O_4P_I = F$ as illustrated in Fig. 9.

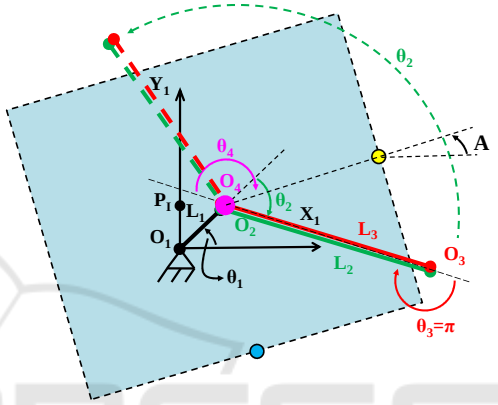

Figure 9: Infinity of configuration corresponding to the point F on the singularity helix.

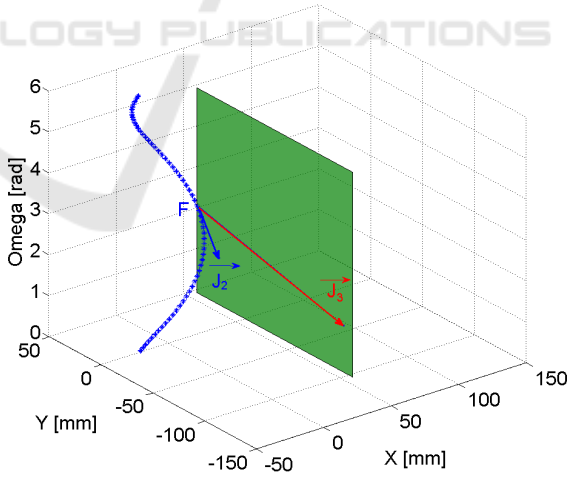

Figure 10: Instantaneous motion of the EE at point F when $\theta_2 = -\pi/4$.

In the location F, the expression of $\vec{J}_2$ is independent of θ_2 or θ_4. It is not the case of the expression of $\vec{J}_3$ which depends explicitly of θ_2 or θ_4. It can be shown that $\vec{J}_2$ is always tangent to the helix, whereas $\vec{J}_3$ changes its size and direction depending on θ_2.

For instance, when $\theta_2 = -\pi/4$, the velocity vector is necessarily in the plane $Y\Omega$ obtained by all linear

SCITEPRESS SCIENCE AND TECHNOLOGY PUBLICATIONS

combinations of $\vec{J}_2$ and $\vec{J}_3$ as displayed in Fig. 10. It is impossible to move in directions that would not be enclosed in the $Y\Omega$ plane.

Now if $\theta_2 = \pi/4$, the vectors $\vec{J}_2$, $\vec{J}_3$ defined a different plane displayed in Fig. 11, which is not vertical anymore. It is only possible to move in directions enclosed in this plane. So theoretically, it is possible from this singular point F to move in every direction but this is not always possible instantly. If the desired direction is not enclosed in the plane resulting from the combinations of $\vec{J}_2$, $\vec{J}_3$, the robot has to maneuver and change the angles θ_2 and θ_4 keeping $\theta_2 + \theta_4 = -\pi/4$ so that the EE still lies at the point F but the direction of $\vec{J}_3$ changes to be in the final desired plane where the EE has to move.

A projection of the singularity surface and curve in the XY plane is presented in Fig. 12. The distance $R_3 = O_4P_I = 21.21\,[mm]$ is already known. Fig. 13 displays the two configurations used to compute R_1 and R_2, minimum and maximum radius of the projected surface. Results based on Fig. 13 are $R_1 = D_1 + D_2 = L_2 + L_3 - O_2P_I = 120 + 120 - 21.21 = 218.79\,[mm]$ and $R_2 = D_4 + D_3 = L_2 + L_3 + O_2P_I = 120 + 120 + 21.21 = 261.21\,[mm]$. It can be clearly seen in Fig. 12 where the workspace of the platform $a \times a = 300\,[mm] \times 300\,[mm]$ is projected, that the workspace was designed to avoid the boundary singularities. But the helix singularity curve is definitely inside the workspace and we have to take this into account.

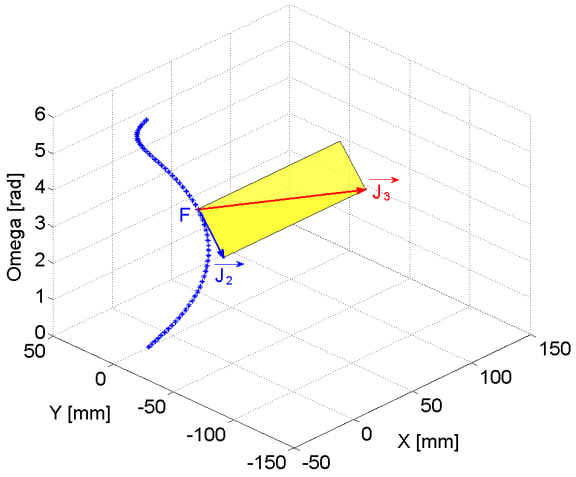

Figure 11: Instantaneous motion of the EE at point F when $\theta_2 = \pi/4$.

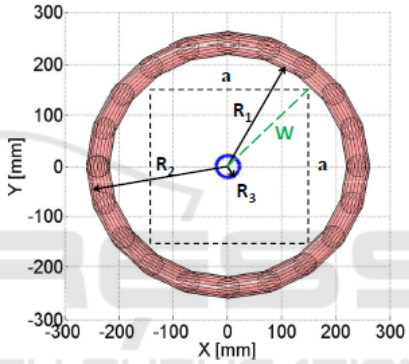

Figure 12: A projection of the singularity surface and curve in the XY plane in the non-redundant case.

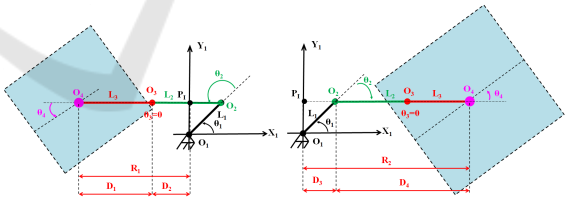

Figure 13: The configuration corresponding of the minimum radius R_1 in the left and the other one corresponding of the maximum radius R_2 in the right.

3.2.2 Redundant Case

In the case of a redundant robot $m > n$, the Jacobian matrix $\overset{(2)}{J}(\theta)$ is not square. Singularities correspond to $det(\overset{(2)}{J}(\theta) \times \overset{(2)}{J}(\theta)^T) = 0$. This equation can be expanded using the Cauchy-Binet formula introducing the $p = (n,m)$ minors Q_k of maximum size extracted from matrix J:

$$det(\overset{(2)}{J}(\theta) \times \overset{(2)}{J}(\theta)^T) = \sum_{k=1}^{p} (det(Q_k)) \times (det(Q_k^T)) = \sum_{k=1}^{p} (det(Q_k))^2 \quad (27)$$

In our case: $m = 4$ and $n = 3$, and the equation implies that the determinant of all minors is nil:

$$det(\overset{(2)}{J}(\theta) \times \overset{(2)}{J}(\theta)^T) = 0 \Rightarrow (\forall k = 1:4), det(Q_k) = 0 \quad (28)$$

The solutions of these equations is a set of four solutions:

1. $S_3 = \{\theta_2 = 0, \theta_3 = 0\}$: the second and third arms are fully stretched out. The singularity surface is obtained for $-\pi \leq \theta_1 \leq \pi$ and $-\pi \leq \theta_4 \leq \pi$ and displayed in Fig. 14. This surface corresponds to the boundary of the workspace. The configuration of the platform for the point M where $\{\theta_1 = -1.88, \theta_2 = 0, \theta_3 = 0, \theta_4 = -0.31\}$ and belonging to this singularity surface is also displayed.

2. $S_4 = \{\theta_2 = \pm\pi, \theta_3 = 0\}$: the second arm is fully

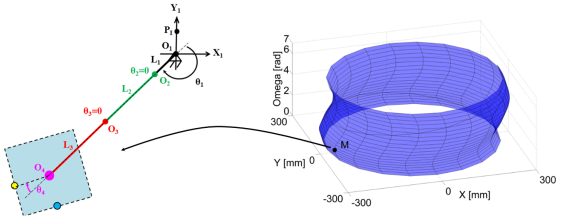

Figure 14: Singularity surface when $S_3 = \{\theta_2 = 0, \theta_3 = 0\}$.

folded back on itself and the third arm is fully stretched out. The singularity surface is obtained for $-\pi \leq \theta_1 \leq \pi$ and $-\pi \leq \theta_4 \leq \pi$ and displayed in Fig. 15. This surface does not correspond to the boundary of the workspace but lies in the interior of the workspace. The configuration of the platform for the point N where $\{\theta_1 = 1.25, \theta_2 = \pi, \theta_3 = 0, \theta_4 = 1.88\}$ and belonging to this singularity surface is also displayed.

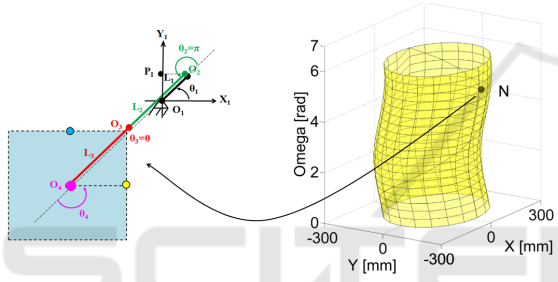

Figure 15: Singularity surface when $S_4 = \{\theta_2 = \pm\pi, \theta_3 = 0\}$.

3. $S_5 = \{\theta_2 = 0, \theta_3 = \pm\pi\}$: the second arm is fully stretched out and the third arm is fully folded back on itself. The singularity surface is obtained for $-\pi \leq \theta_1 \leq \pi$ and $-\pi \leq \theta_4 \leq \pi$ and displayed in Fig. 16. This surface does not correspond to the boundary of the workspace but lies in the interior of the workspace. The configuration of the platform for the point O where $\{\theta_1 = -2.88, \theta_2 = 0, \theta_3 = \pi, \theta_4 = 1.25\}$ and belonging to this singularity surface is also displayed.

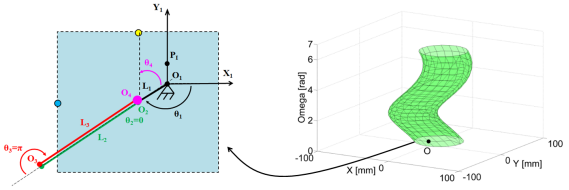

Figure 16: Singularity surface when $S_5 = \{\theta_2 = 0, \theta_3 = \pm\pi\}$.

4. $S_6 = \{\theta_2 = \pm\pi, \theta_3 = \pm\pi\}$: the second arm is fully folded back on itself and the third arm is also fully folded back on itself. The singularity surface is obtained for $-\pi \leq \theta_1 \leq \pi$ and $-\pi \leq \theta_4 \leq \pi$ and displayed in Fig. 17. This surface does not correspond to the boundary of the workspace but lies in the interior of the workspace. The singularity surface of case 3 and 4 are in fact identical. The configuration of the platform for the point P where $\{\theta_1 = -1.57, \theta_2 = \pi, \theta_3 = \pi, \theta_4 = 1.25\}$ and belonging to this singularity surface is also displayed.

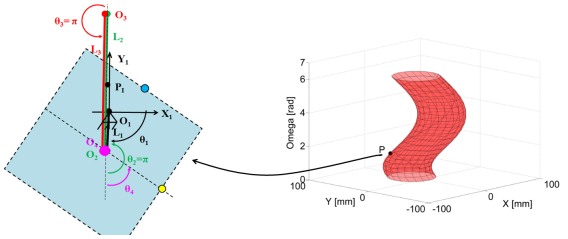

Figure 17: Singularity surface when $S_6 = \{\theta_2 = \pm\pi, \theta_3 = \pm\pi\}$.

Let us analyze each of these cases and draw the singularity surfaces which are displayed in Fig. 18. Concerning S_3, the second and third arms are fully stretched out. The singularity surface in blue is obtained for $-\pi \leq \theta_1 \leq \pi$ and $-\pi \leq \theta_4 \leq \pi$. Regarding S_4, the second arm is fully folded back on itself and the third arm is fully stretched out. The singularity surface in yellow is obtained for $-\pi \leq \theta_1 \leq \pi$ and $-\pi \leq \theta_4 \leq \pi$. Concerning S_5, the second arm is fully stretched out and the third arm is fully folded back on itself. The singularity surface in red is obtained for $-\pi \leq \theta_1 \leq \pi$ and $-\pi \leq \theta_4 \leq \pi$. Versus S_6, the second arm is fully folded back on itself and the third arm is also fully folded back on itself. The singularity surface are identical with former case S_5 in red for $-\pi \leq \theta_1 \leq \pi$ and $-\pi \leq \theta_4 \leq \pi$.

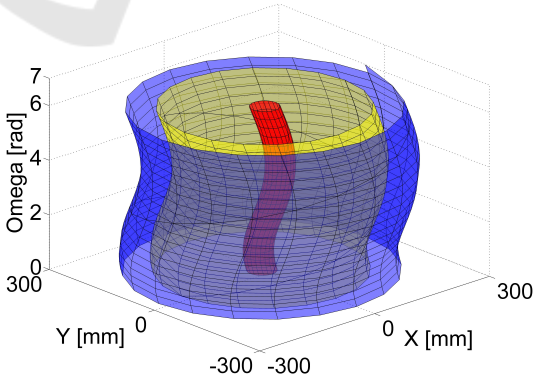

Figure 18: Singularity surfaces when the robot is redundant.

3.2.3 Discussion about the Kinematic Induced Constraints

Considering the non-redundant case, the trajectory of the robot EE can cross the singularity helix without

causing any specific problem if the trajectory is differentiable. Indeed, the tangent to the direction of the arrival defines the velocity vector and this same direction can be used to leave the singularity, because the velocity will necessarily be inside the tangent plane defined by $\vec{J}_2$ and $\vec{J}_3$. However the drawbacks of singularity will always be present in the vicinity of the singularity, if the trajectory followed by the EE is close to the helix, then the velocity of the joints would be important.

In the redundant case, the analysis is different. The singularity surfaces can be avoided because in this case, the inverse kinematic function leads to an infinity of solutions for each point inside the workspace. Because of redundancy, it is always possible to choose a set of input coordinates (θ_1,..., θ_4) to avoid crossing a singular configuration. Of course, this implies implementing this constraint in the control loop, using the manipulability index for instance. If following a given trajectory the robot has unfortunately reached the singularity surface, the velocity is then constrained to be in the plane tangent to the singularity surface, and the robot loses instantly one dof in the (X,Y,Ω) space. This can cause great problems and sometimes the EE would not be able to follow the planned trajectory. Indeed let us study the case when the trajectory crosses the singularity surface without arriving in the tangent plane. If the control is well done in the (θ_1,..., θ_4) space, the singular configurations are avoided and in fact the singularity surface does not exist. The robot EE can follow the trajectory without any problem. If the control does not manage to avoid the singularity, and a singular configuration in the space (θ_1,..., θ_4) occurs just when the EE arrives on the potential singularity surface in (X,Y,Ω). Then necessarily, the EE has to leave the singular point with a velocity vector in the plane tangent to this surface. The robot will not be able to follow the initial trajectory anymore.

4 CONCLUSION

In this paper, the singularity loci of an XY-Theta platform held by a serial manipulator have been analyzed in details. The high precision performances of the platform result from the proximity of singularities, but require to identify the loci and analyze the kinematic problems that could occur. This analysis is done in two steps: firstly, when the robot is non-redundant, an unusual case is brought to light where the surface singularity degenerates into an helix. This singularity helix does not prevent the robot EE to follow a differentiable trajectory, but some usual drawbacks are encountered if the trajectory is close to the helix. Secondly, the four joints are used to control the robot and the potential singularity loci are identified. Here, if the control manages to avoid the singular configurations in the (θ_1,..., θ_4) space, then the robot can move inside the dexterous workspace without any restrictions. Otherwise, if unfortunately, the singular configuration in (θ_1,..., θ_4) space is encountered while the EE lies on the singularity surfaces, then the robot EE will not be able to follow the trajectory anymore. This is why it is of major importance to implement a control strategy taking into account a certain distance towards singularity configurations.

Our future work will now be to implement such strategies in our control algorithms to be able to follow any trajectory in the workspace.

REFERENCES

Abdel-Malek, K. and Yeh, H.-J. (2000). Crossable surfaces of robotic manipulators with joint limits. *ASME, Journal of Mechanical Design*, 122, No. 1,:52–61.

Bohigasa, O., Manubensa, M., and Rosa, L. (2013). Singularities of non-redundant manipulators: A short account and a method for their computation in the planar case. *Mechanism and Machine Theory*, 68:1?17.

Brethé, J. F. (2011a). Granular stochastic space modeling of robot micrometric precision. In *IROS*, pages 4066–4071.

Brethé, J. F. (2011b). High precision motorized micrometric table. FR2011/02184, Patent.

Brethé, J. F., Hijazi, A., and Lefebvre, D. (2013). Innovative xy-theta platform held by a serial redundant arm. *ECMSM*, pages 146–151.

Chablat, D. and Wenger, P. (1998). Working modes and aspects in fully parallel manipulators. *Robotics and Automation*, 3:1964 – 1969.

Gosselin, C. and Angeles, J. (1990). Singularity analysis of closed-loop kinematic chains. *IEEE Transactions on Robotics*, 6:281–290.

Hijazi, A., Brethé, J. F., and Lefebvre, D. (2014). Characterization of repeatability of xy-theta platform held by robotic manipulator arms using a camera. *ICINCO*, pages 421–427.

Hijazi, A., Brethé, J. F., and Lefebvre, D. (Accepted in February 2015). Design of an xy-theta platform held by a planar manipulator with four revolute joints and evaluation of its precision. *Robotica*.

Kao, C.-C., Wu, S.-L., and Fung, R.-F. (2007). The 3rps parallel manipulator motion control in the neighborhood of singularities. *in Proceedings of the International Symposium on Industrial Electronics, Mechatronics and Applications*, 1:165?179.

Khalil, W. and Dombre, E. (2002). *Modeling, Identification and Control of Robots*.

Merlet, J. P. (1989). Singular configurations of parallel manipulators and grassmann geometry. *International Journal of Robotics Research*, 8(5):45–56.

Merlet, J.-P. (2006). *Parallel Robots*. 2nd Ed. Springer.

Mi, Z., Yang, J., Kim, J., and Malek, K. A. (2011). Determining the initial configuration of uninterrupted redundant manipulator trajectories in a manufacturing environment. *Robotics and Computer-Integrated Manufacturing*, 27:22–32.

Tsai, L.-W. (1999). *Robot Analysis: The Mechanics of Serial and Parallel Manipulators*. John Wiley & Sons.

Wenger, P. (2007). Cuspidal and noncuspidal robot manipulators. *Robotica*, 25(6):717–724.

Zlatanov, D., Fenton, R. G., and Benhabib, B. (1995). A unifying framework for classification and interpretation of mechanism singularities. *Transactions of the ASME*, 117:566–572.

SCITEPRESS
SCIENCE AND TECHNOLOGY PUBLICATIONS